Anisoplanatic adaptive optics in parallelized laser scanning microscopy

Pozzi, Paolo; Smith, Carlas; Carroll, Elizabeth; Wilding, Dean; Soloviev, Oleg; Booth, Martin; Vdovin, Gleb; Verhaegen, Michel

DOI
10.1364/OE.389974

Publication date
2020

Document Version
Final published version

Published in
Optics Express

Citation (APA)
Pozzi, P., Smith, C., Carroll, E., Wilding, D., Soloviev, O., Booth, M., Vdovin, G., & Verhaegen, M. (2020). Anisoplanatic adaptive optics in parallelized laser scanning microscopy. *Optics Express*, *28*(10), 14222-14236. https://doi.org/10.1364/OE.389974

Research Article | Vol. 28, No. 10 / 11 May 2020 / Optics Express 14222
Optics EXPRESS

Anisoplanatic adaptive optics in parallelized laser scanning microscopy

PAOLO POZZI,[1,2,*] CARLAS SMITH,[1,3,4,5] ELIZABETH CARROLL,[4] DEAN WILDING,[1] OLEG SOLOVIEV,[1,6] MARTIN BOOTH,[3,5] GLEB VDOVIN,[1,6] AND MICHEL VERHAEGEN[1]

[1]*Delft Centre for Systems and Control, Delft University of Technology, Mekelweg 2, 2628 CD Delft, The Netherlands*
[2]*Department of Biomedical, Metabolic and Neural Sciences, Center for Neuroscience and Neurotechnology, University of Modena and Reggio Emilia, Modena, Italy*
[3]*Centre for Neural Circuits and Behaviour, University of Oxford, Mansfield Road, Oxford OX1 3SR, United Kingdom*
[4]*Department of Imaging Physics, Delft University of Technology, Lorentzweg 1, 2628 CJ Delft, The Netherlands*
[5]*Department of Engineering Science, University of Oxford, Parks Road, Oxford OX1 3PJ, United Kingdom*
[6]*Flexible Optical B.V., Polakweg 10-11, 2288 GG Rijswijk, The Netherlands*
[*]*paolo.pozzi87@unimore.it*

Abstract: Inhomogeneities in the refractive index of a biological microscopy sample can introduce phase aberrations, severely impairing the quality of images. Adaptive optics can be employed to correct for phase aberrations and improve image quality. However, conventional adaptive optics can only correct a single phase aberration for the whole field of view (isoplanatic correction) while, due to the highly heterogeneous nature of biological tissues, the sample induced aberrations in microscopy often vary throughout the field of view (anisoplanatic aberration), limiting significantly the effectiveness of adaptive optics. This paper reports on a new approach for aberration correction in laser scanning confocal microscopy, in which a spatial light modulator is used to generate multiple excitation points in the sample to simultaneously scan different portions of the field of view with completely independent correction, achieving anisoplanatic compensation of sample induced aberrations, in a significantly shorter time compared to sequential isoplanatic correction of multiple image subregions. The method was tested in whole *Drosophila* brains and in larval *Zebrafish*, each showing a dramatic improvement in resolution and sharpness when compared to conventional isoplanatic adaptive optics.

1. Introduction

Adaptive optics(AO) is a method of growing popularity for the correction of phase aberrations in optical systems. Optical microscopes can particularly benefit from AO, as most samples of interest for life sciences are thick and inhomogeneous, introducing significant phase aberrations to light propagating through them. Implementations of AO have been reported for many of the most popular fluorescence microscopy techniques in life sciences [1]. In the classical implementation of AO [2], an adaptive optical element (AOE), such as a deformable mirror, or a liquid crystal spatial light modulator, is generally introduced in the back aperture plane of the system. In order to improve the image quality, the difference between the phase modulation introduced by the AOE and the sample induced phase aberration should be minimized. The main limitation in this approach is due to the fact that a AOE in the pupil plane of an optical system is only capable of applying an isoplanatic correction, meaning the same two-dimensional pupil plane correction is applied to all points within the field of view. As a consequence, correction of aberrations can either be performed optimally on a small subregion of the field of view, or alternatively only the

#389974 https://doi.org/10.1364/OE.389974
Journal © 2020 Received 26 Feb 2020; revised 30 Mar 2020; accepted 1 Apr 2020; published 27 Apr 2020

Optics EXPRESS

average aberration can be corrected. The anisoplanatic nature of sample-induced aberrations requires independent correction for each point of the field of view, which can not be achieved with a single AOE, as schematically represented in Fig. 1, panel a.

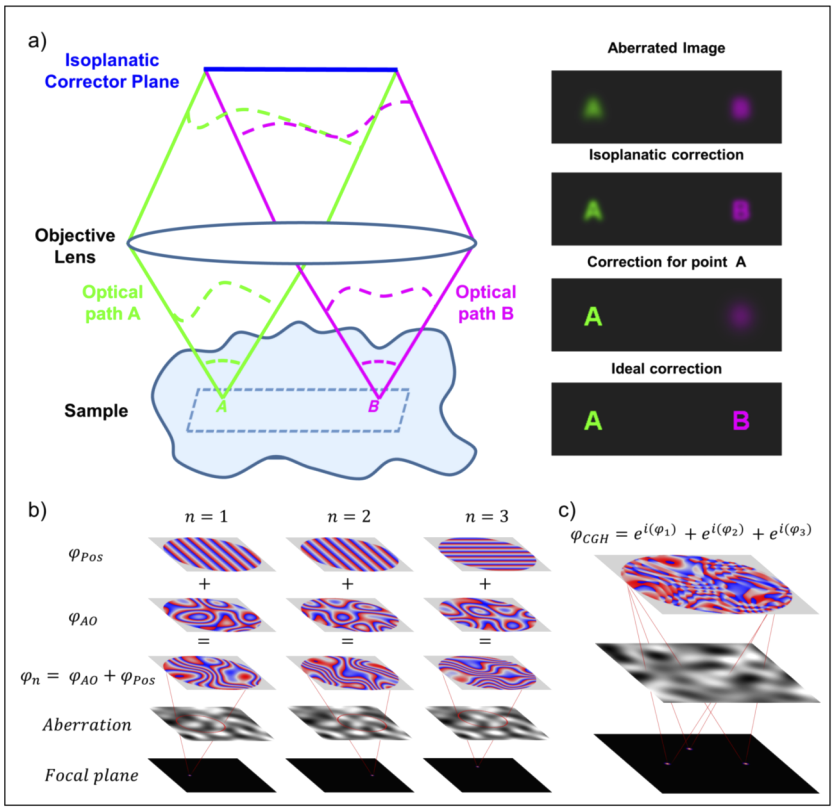

Fig. 1. Anisoplanatic aberrations and correction approach. a Light from different parts of the field of view travel through different sections of the sample, and are therefore affected by different aberrations, which can not be compensated completely by a single corrector in the pupil plane. **b** phase patterns generating single corrected spots in different locations in the sample. It should be apparent that the corrected phase aberration varies depending on the spot location. **c** Multispot hologram with independent spots correction. The hologram is a complex sum of the phase patterns generating the single corrected spots. It is crucial to notice that all correction patterns are defined over the full size of the pupil, therefore exploiting the full resolution of the corrector.

A similar problem is encountered in astronomy and ophthalmology, where multiple layers of inhomogeneous medium can affect the image quality, and the most common approach to correction is the use of multiple AOE conjugated to different optical planes [3–5]. This approach, to the knowledge of the authors has never been reported in fluorescence microscopy applications, possibly due to the homogeneous nature of aberrations induced by most microscopy samples, rarely organized in layers. Three main approaches have been previously reported to attempt compensation of anisoplanatic aberrations: sequential correction [6], multiplexed pupil [7] and conjugate adaptive optics [8–10]. Sequential correction methods are based on correction and acquisition of small subregions of the field of view of the microscope, which are then combined to form the entire image. This method is extremely time consuming, and has in fact only been reported for lattice light-sheet microscopy, which can provide extremely high acquisition frame

Optics EXPRESS

rates, and only through a complex wavefront sensing setup based on multiphoton excited guide stars. The approach would be slow to the point of unfeasibility for sensorless correction on a laser scanning microscope (see section 4.). Multiplexed pupil approaches are based on the use of a high resolution AOE, which is split in multiple subregions, each correcting a different area of the field of view. An inevitable limitation of this approach is due to the required tradeoff between the number of independently corrected subregions and the resolution available for each sub-area of the AOE. Due to this, and the technical difficulty of splitting the optical paths, such an approach has only be proven for the correction of 9 independent regions of the field of view. Finally, in conjugate AO, the AOE conjugation plane can be dynamically positioned in any plane between the objective pupil plane and the focal plane. However, while greatly improving the effectiveness of aberration correction, this approach only provides complete correction if the aberration is mostly confined to a 2D plane [10]. Moreover, the variable magnification of such a system imposes a tradeoff between the size of the independently corrected patches and the order of the aberration.

This paper presents a novel approach to anisoplanatic correction in laser scanning confocal fluorescence microscopy, allowing for spatially varying aberration correction of the excitation light throughout the field of view by parallelized acquisition of multiple isoplanatic patches with an array of independently corrected foci generated by a spatial light modulator (SLM). Emission light is corrected isoplanatically with a deformable mirror (DM). The method allows simultaneous and independent aberration correction in up to hundreds of subregions of the field of view, without the tradeoffs between the number of independently corrected patches and the resolution of the applied phase correction that characterizes conjugate adaptive optics methods. In particular, the results presented in section 6., show independent correction of 64 subregions, each for aberrations defined over the full 512x512 pixels of the employed AOE.

2. Method description

This paper introduces a new imaging method, named Laser Scanning Fluorescence Microscopy with Anisoplanatic Correction of Excitation (LSFM-ACE). The confocal imaging principle of an LSFM-ACE microscope is equivalent to that of a conventional laser scanning confocal microscope, where excitation light is focused in the sample in a diffraction limited spot, and the confocal fluorescence emission is filtered through a pinhole. Unlike a regular laser scanning microscope, LSFM-ACE scans a regular lattice of excitation spots, and employs individual pixels of a pixelated detector as a regular lattice of pinholes. An image can be acquired by raster scanning the spots with width and height equal to the separation distance between focal points of the lattice, so that each spot scans an independent rectangular subregion of the total field of view. A DM in the shared path between excitation and fluorescence light is used to perform both scanning and traditional isoplanatic sensorless aberration correction. An anisoplanatic correction is added to the excitation light through computer generated holography. In order to generate a lattice of independently-corrected spots, an SLM, conjugated to the back aperture of the system, is used to modulate the phase of excitation. The possibility of generating multiple diffraction limited spots through a strongly anisoplanatic aberration by means of a high order phase pattern has been previously proven both through strongly scattering materials [11] and multimode optical fibers [12]. These techniques however require global optimization of the full pattern or identification of the transmission matrix of the medium, both complex and lengthy procedures which could not be applied on-the-fly for every new sample, especially if imaging at multiple depths, each requiring independent correction. In this paper we propose, instead, to correct for the aberrations of less complex materials, such as conventional microscopy samples, through the use of a point cloud computer generated hologram (CGH). In particular, In order to generate N spots, each located at positions x'_n, y'_n and each corrected by a pupil aberration $\phi_{AO,n}$,

Optics EXPRESS

the CGH can be computed as:

$$\phi_{CGH} = \arg\left(\sum_{n=1}^{N} e^{i(\phi_{POS,n}+\phi_{AO,n}+\theta_n)}\right), \tag{1}$$

where θ_n are constant phase terms, which do not influence the phase correction of the $n-$th spot, and can be optimized to improve the hologram quality with a variety of algorithms [13,14]. $\phi_{POS,n}$ is a displacement phase pattern

$$\phi_{POS,n}(x,y) = \frac{2\pi}{\lambda f}(xx'_n + yy'_n), \tag{2}$$

where λ is the excitation wavelength, and f is the equivalent focal length of the system.

The general principle of independently corrected CGH generation is qualitatively represented in Figure 1 and Algorithm 1.

It is important to notice that, since the complete point spread function of a confocal fluorescence microscope is the product of the excitation light point spread function with the fluorescence emission point spread function [15], correction of the excitation wavefront alone is sufficient for restoring near-optimal resolution. Correction of the isoplanatic aberration of the fluorescence light, while not optimal for all points, can still improve the signal to noise ratio of the acquired image.

Another important implication of Eq. (2) regards the maximum lateral displacement of SLM generated spots, and therefore the maximum field of view achievable with the technique. In particular, given the resolution of the SLM and the pupil diameter, aliasing effects will appear if the phase pattern $\phi_{POS,n}$ has a gradient higher than $\frac{\pi}{pixel}$. It can easily be derived that the maximum displacement x_{max} in a given direction is given by

$$x_{max} = \frac{\lambda f R}{2D} \approx \frac{\lambda R}{4NA} \tag{3}$$

where R is the number of pixels of the SLM along the diameter of the aperture, and D is the aperture diameter. It can therefore be seen that the available field of view is proportional to the wavelength, and inversely proportional to the numerical aperture of the system. It is important to notice that, while SLMs generally have low efficiency (approximately 60% in the reported setup), this does not constitute a problem for this application, as the SLM is exclusively used to modulate excitation light, where the power provided by commercial sources is generally orders of magnitude greatar than the power actually needed for imaging.

3. Sensorless optimization approach

While wavefront sensing based correction of excitation light is possible [16], its implementation in a parallelized focus method would be extremely complex, and exceed the scope of this paper. Instead, a simpler sensorless approach was developed.

The sensorless correction of aberrations in LSFM-ACE was performed in two steps. Firstly, the DM is employed to perform conventional isoplanatic adaptive optics, anisoplanatic correction of all excitation spots is then performed through the SLM.

Isoplanatic correction can be performed with any previously reported method. For the results presented in this paper, the optimal model based method previously developed by the authors [17] was used. For this specific optimization procedure, the second moment of the average spatial distribution of the camera images of spots is used as a metric. Anisoplanatic correction of a total of N spots requires estimation of a single CGH ϕ_{CGH} simultaneously maximizing N metric functions $\Upsilon_n(\phi)$, each measuring the correction performance in the area scanned by the n-th spot.

Optics EXPRESS

The metric functions $\Upsilon_n(\phi)$ were computed as the average intensities of the N one-dimensional fluorescence intensity signals acquired by using the DM to perform a spiral scan within the area scanned by each spot. A spiral scan was preferred to a raster scan as it allows computation of metric values in a considerably shorter time, while still covering most of the scan area, as opposed to line or circular scanning. For the presented results, the optimization implemented was a parallelized generalization of previously reported [18] methods, consisting of an hill-climb optimization over a gradient orthogonal Lukosz polynomial base.

Algorithm 1 Optimization algorithm

Create initial CGH $\Phi^0_{CGH} = arg\left(\sum_{n=1}^{N} e^{i(\phi_n^0+\theta_n)}\right)$
Perform isoplanatic correction
for $j \leftarrow 1$ to M **do**
  for $a \leftarrow -1$ to 1 **do**
    add isoplanatic aberration aL_j to CGH
    Measure average intensity along spiral scan as in Figure 2 panel **b**
  end for
  Fit intensity traces with Lorentz function as in Figure 2 panel **c** to find maximas $\hat{a}_n^j$
  Update isoplanatic patches corrections $\phi_n^j = \phi_n^{j-1} + \hat{a}_n^j L_j$
end for
Re-compute the values of θ_n with CS-WGS algorithm and update CGH
Acquire raster image as in Figure 2 panel **d**

The optimization is initialized by computing a starting CGH ϕ^0_{CGH} generating a lattice of N uncorrected spots:

$$\phi^0_{CGH} = \arg\left(\sum_{n=1}^{N} e^{i(\phi_n^0+\theta_n)}\right), \tag{4}$$

where θ_n are constant phase terms, computed through the recently presented compressed sensing weighted Gerchberg Saxton algorithm [14], and ϕ_n^0 are the phase patterns generating independently each of the N spots, as reported in Eq. (2). After initialization, the optimization was performed through a hill-climb procedure over a truncated base of M Lukosz polynomials [18] $\{L_1, \ldots, L_M\}$. At the j-th iteration of the algorithm, the metric functions $\Upsilon_n(\phi^{j-1} + aL_j)$ were measured for linearly modulated values of the amplitude a, in order to solve the n one-dimensional maximization problems:

$$\max_{a_n^j} \Upsilon_n(\phi^{j-1} + a_n^j L_j)\,, \tag{5}$$

by fitting the functions Υ_n with Lorentzian models [18], in order to estimate the amplitudes $\hat{a}_n^j$ maximizing each function. A new CGH was then computed as:

$$\phi^j_{CGH} = \arg\left(\sum_{n=1}^{N} e^{i(\phi_n^j+\theta_n)}\right), \tag{6}$$

where:

$$\phi_n^j = \phi_n^{j-1} + \hat{a}_n^j L_j\,, \tag{7}$$

and the procedure is performed until $j = M$.

It is to be noticed that the values of θ_n are not re-optimized at each step of the procedure in order to reduce the total correction time. This can reduce the uniformity of intensity between spots during optimization, but has no effects on the estimation of the values of the correction

Optics EXPRESS

coefficients $\hat{a}_n^j$. After the M-th iteration, the values of θ_n were recalculated through the compressed sensing weighted Gerchberg Saxton algorithm to ensure uniform intensity between spots, and the system was ready to acquire an aberration corrected image. The described optimization approach was chosen due to its simplicity in implementation for simultaneous optimization of multiple functions. Better performances in optimization speed could, in principle, be achieved through the development of parallelized versions of other algorithms.

4. Correction and acquisition speed

Correction speed. The main speed advantage of LSFM-ACE compared to a traditional laser scanning microscope with isoplanatic correction lies in its parallelized correction. A traditional system would need to correct aberrations in each subregion sequentially. Supposing to employ a similar, very widespread [18,19], hillclimb optimization algorithm for sensorless correction, the optimization time for a single correction subregion would be roughly similar to the total correction time of LSFM-ACE. The speed improvement provided by LSFM-ACE is therefore proportional to the number of points in the scanned array, which in the case of the reported images is 64-fold. A traditional system, due to its single-point scanning nature would make sensor-based correction easier, but unless multiphoton excitation is employed, an independent physical fluorescent guide star (e.g., a fluorescent microbead) would be required in each corrected subregion. Ultimately, a similar approach is impractical, has never been reported on laser scanning systems, and the only known application for fluorescence microscopy is on a lattice light-sheet microscope with a multiphoton-excited guide star system employing an EMCCD based Shack-Hartmann detector [6]. Due to its complexity and cost, a sensorless approach still remains a viable and simpler alternative for anisoplanatic correction.

Image acquisition speed. When not limited by the signal to noise ratio, traditional laser scanning confocal microscopes are limited in acquisition speed by the scanning frequency of its scanner. While extremely fast resonant scanners are capable of up to 8 kHz line acquisition frequency, their non-uniform scanning speed over the field of view generally limits their employment to live imaging applications where the speed of acquisition is considered far more important than the image quality. More conventional galvanometric scanners can achieve line acquisitions frequencies up to a few hundred Hz. Supposing that, in order to obtain anisoplanatic correction as in LSFM-ACE, a traditional microscope with isoplanatic adaptive optics would be employed to acquire an $N \times N$ pixels image as a mosaic of 64 images, each with $N/8 \times N/8$ resolution, with a scanner of frequency f, the total frame time would be equal to $8N/f$. Image acquisition speed in LSFM-ACE is limited by the frame rate f of the employed camera. For each frame acquired by the camera, 64 pixels of the final image are acquired. Consequently, the total frame time for a $N \times N$ pixels image is $\frac{N^2}{64f}$. Considering the frame rate of an sCMOS camera is similar to the line scanning speed of a traditional confocal, LSFM-ACE is faster than a traditional confocal for low sampling images, and is approximately $N/512$ times slower for high resolution images, in the assumption of using a 64 spots square array. Nonetheless, this theoretical difference is mitigated by the fact that the pixel dwell time for LSFM-ACE is fixed at the camera exposure time, while increasing the sampling in a traditional confocal inevitably reduces the pixel dwell time, and therefore the signal to noise ratio. As an example, in order to acquire images of 800×800 pixels like those reported in this paper, a traditional confocal would be less than twice as fast as LSFM-ACE, while the pixel dwell time of a traditional confocal would be $2.5\mu s$ which isn't viable even for extremely bright samples and would generally require a reduction in the scanning speed or the averaging of multiple frame to obtain similar performances to LSFM-ACE.

Optics EXPRESS

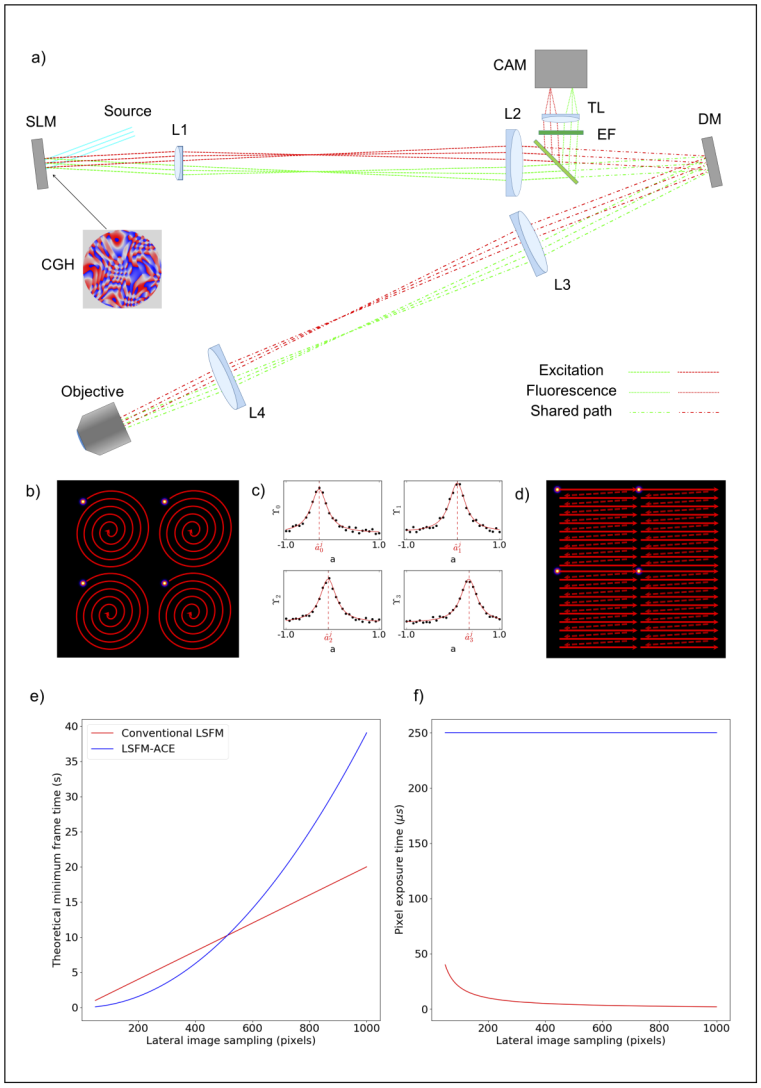

Fig. 2. Method description and performance a Schematic representation of the optical setup, reporting the optical paths for two spots at the edges of the field of view, represented in green and red. Displacement between spots is exaggerated to aid readability. Excitation light (Source) was modulated by the SLM with the computed hologram (CGH). The SLM plane was conjugated by a telescope (L1,L2) to the DM plane. A second telescope (L3,L4) conjugated the DM to the back aperture of the objective. Fluorescence light propagated the opposite direction, was descanned by the DM, filtered by a dichroic and emission filter set (EF) and focused by a short focal tube lens (TL) on the camera detector (CAM). **b** Schematic representation of the intensity distribution and scanning path at the sample plane for a 4 spot LSFM-ACE, with scanning path for the acquisition of metric values. **c** Simulated examples of Lorentzian fits for the estimations of maximas of a given coefficient. **d** Scanning path for the final image acquisition. **e** Comparison of minimum achievable frame time for LSFM-ACE correcting 64 subregions with a 400Hz camera and sequential correction with a traditional confocal microscope scanning at 400Hz **e** Pixels exposure times for LSFM-ACE and sequential correction with a traditional confocal microscope, under the same assumptions as in panel e.

Optics EXPRESS

5. Experimental setup

A custom LSFM-ACE microscope was realized for the imaging of green fluorophores. A schematic representation of the system is reported in Fig. 2, panel a. Excitation light was provided by a single mode, solid state laser at $488nm$ (Sapphire 488, Coherent) expanded to a beam waist of $10mm$ in order to provide uniform illumination of the SLM surface. The SLM employed (P512-0532, Meadowlark Optics) had resolution of 512×512 pixels on a surface area of $7 \times 7mm$, with a refresh rate of $200Hz$.

A 1.5× telescope of two achromatic doublets of focal lengths 100 and $150mm$ respectively (AC508-100-A-ML and AC508-150-A-ML, Thorlabs) was used to conjugate the surface of the SLM to the surface of the DM. A vertically mounted thin copper wire was used in the focal plane of the first lens of the telescope to mask the zeroth order of diffraction of the SLM. In this configuration, the wire did not block any of the generated spots, as long as they were organized in a lattice of even number along the horizontal axis. A 69 actuators voice coil based DM (DM-69, Alpao) was used both for isoplanatic aberration correction and scanning, therefore preventing the need for an additional scanning device.

A 0.83× telescope of two achromatic doublets of focal lengths 180 and $150mm$ respectively (AC508-180-A-ML and AC508-150-A-ML, Thorlabs) was used to conjugate the surface of the DM to the back aperture of the microscope objective (63×, $1.4N.A.$, oil immersion, Leica and 10×, $0.4N.A.$, dry, Leica). A dichroic mirror ($496nm$ shortpass, Semrock) was positioned in infinity space between the DM and the second lens of the telescope conjugating SLM and DM. Fluorescence light was further filtered by a bandpass filter (MF525-39, Thorlabs). A $50mm$ achromatic lens (AC254-050-A-ML, Thorlabs) was used to focus images of the spots to an sCMOS camera (Optimos, QImaging). Single pixels of the cameras were used as virtual pinholes to filter out of focus emission as in a traditional confocal laser scanning microscope. From each camera frame a single pixel of the final confocal image was acquired for each excitation spot. In order to correct for aberrations due to the optical system itself, a baseline correction was performed by imaging a test sample of fixed bovine pulmonary artery endothelial cells with Bodipy staining on α-tubulin (Fluocells slide 2, Invitrogen). Due to the very thin nature of the sample, such baseline correction was assumed to be the system aberration, and applied to all acquired images. In order to prove the uniformity of system aberrations correction, an image of sub-diffraction limit microspheres was acquired without correction, measuring the point spread function width throughout the field of view.

6. Results

The system was tested on fixed whole *Drosophila melanogaster* brains, expressing green fluorescent protein on isolated neurons (see methods). A lattice of 8×8 spots was generated with the SLM, each scanning a $11 \times 11\mu m$ area in a 100×100 pixels raster pattern, achieving sampling at the objective diffraction limited resolution. Pixel intensities were sampled by the camera at $400Hz$. This resulted in images with a field of view of $88 \times 88\mu m$, close to the limit derived by Eq. (3), with a resolution of 800×800 pixels with an acquisition time of approximately $30s$. Isoplanatic adaptive optics was performed on a set of 24 gradient orthogonal [17] mirror modes. Correction time for a single image was approximately $5s$. Anisoplanatic correction was performed as described in section 3.. The first 24 Lukosz polynomials, excluding tip,tilt and defocus, were used as modes for correction. While the SLM was capable of correcting much higher order aberration, a set of 24 low order aberrations was chosen in order to ensure optimization times compatible with experimental needs. Moreover, this ensured that anisoplanatic and isoplanatic corrections were performed on aberrations of similar order, ensuring that any improvement in image quality was due to anisoplanatic correction, and not to correction of higher order aberrations. The metric was acquired on spiral scans each performed during a single camera exposure of $10ms$. 29 spiral scans were acquired for each mode. The specific number

Optics EXPRESS

of scans was decided empirically, as we found it represented, for the reported applications, the best tradeoff between correction speed and quality. In experimental conditions, anisoplanatic correction of a single plane required approximately 25 seconds, including the final compressed sensing weighted Gerchberg-Saxton optimization step.

In order to compare performances between the uncorrected system, the isoplanatic and the anisoplanatic correction, each image was acquired first without correction, then with isoplanatic correction, and finally after anisoplanatic optimization. This was done so that, in case of appearence of photobleaching, no unfair advantage in the comparison would be given to the presented method. Nonetheless, no significant photobleaching was observed during the acquisition of the images reported in this paper.

Figure 3 reports example images acquired without correction, with isoplanatic correction, and with LSFM-ACE. It can be noticed that, while traditional isoplanatic correction enhanced the quality and sharpness of the image, the introduction of an anisoplanatic correction component on the excitation greatly improves contrast, and allowed the resolution of details of the image which would simply be lost due to aberrations.

Panels j and k of Fig. 3 report the final corrected isoplanatic and anisoplanatic aberrations. It can be observed that the isoplanatic component has relatively low order, while the single corrections of individual patches in the LSFM-ACE image present high order modes and widely vary across the field of view. In order to evaluate performance of the correction in three dimensional imaging, and to prove that image quality improvement in the results presented are not due to refocusing, axial scans of another specimen from the same line were acquired over $40\mu m$ thickness, updating the correction every $5\mu m$. Panels d to i of Fig. 3 report maximum intensity projections of the images both horizontally and axially. It can be observed how isoplanatic adaptive optics can not recover the full details in the image which are only visible after anisoplanatic correction, especially at the deeper planes.

In order to estimate the improvement in image quality, all images were acquired twice, and Fourier ring correlation analysis was performed over each corrected patch. The results are reported in Fig. 4, showing how resolution was improved by LSFM-ACE compared to isoplanatic correction, with a more than 2-fold gain in resolution in selected patches, and an increase of 50% in the extent of the area imaged with lateral resolution under 500**nm** and in the extent of the volume imaged with axial resolution under 800**nm**.

In order to better highlight the correction capabilities of LSFM-ACE, a second set of images was acquired on a larger sample with more dramatic aberrations present. The sample of choice was a Tg(flk1:egfp) zebrafish embryo, which exhbits GFP expression in blood vessels, fixed at 4 days post fertilization. The sample was mounted in 2 % agarose gel within a square borosilicate glass capillary, with 200 μm walls and 1 mm inner side. The sample was imaged with a 10× magnification, $0.4 N.A.$ dry objective (Leica), underfilling the aperture with excitation light to $0.24 NA$, as the field of view increase, determined by Eq. (3),allows imaging of the full embryo head. A maximum intensity projection of the images is shown in Fig. 5.

The high index mismatch due to the dry objective, together with the small size of the isoplanatic patches due to the wide field of view, demonstrate the gap in performance between conventional AO and LSFM-ACE. In particular, LSFM-ACE is able to retrieve details of small vessels in the optic tectum, where the curvature of the fish introduces significant aberrations.

Optics EXPRESS

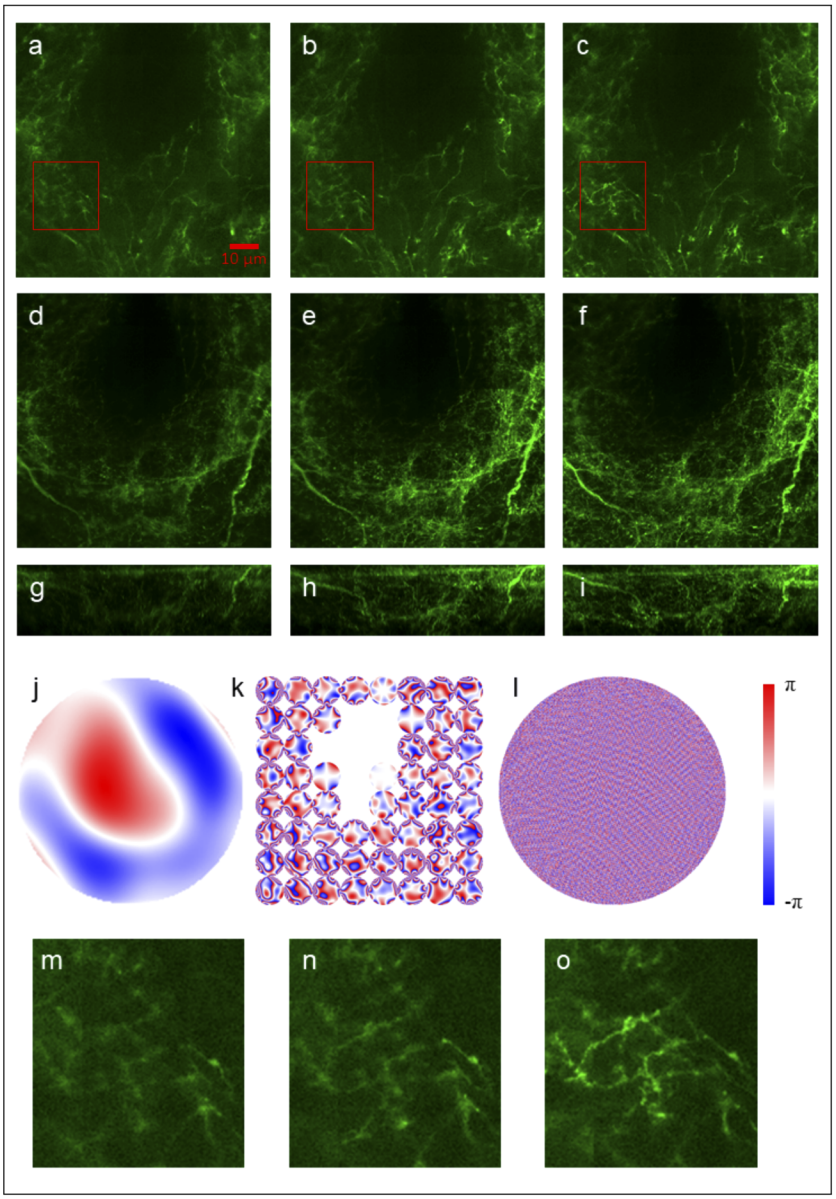

Fig. 3. Image correction comparison. Example of image acquired with LSFM-ACE, all images of the same sample are on the same intensity scale. **a, b, c** Image at approximately 15 μm depth respectively without adaptive optics, corrected with isoplanatic adaptive optic and with anisoplanatic correction of excitation. **d, e, f** maximum intensity projection, of a 30μm thick stack of the same sample of panels a, b, c. **g, h, i** x-z maximum intensity projection of the same stacks of panels d, e, f. **j** Isoplanatic correction applied with the DM on the plane imaged in b and c. **k** Individual correction of the 8×8 patches corrected in panel c. **l** SLM hologram generating the anisoplanatically corrected hologram in c. **m, n, o)** details from the red highlighted areas in a, b, c.

Optics EXPRESS

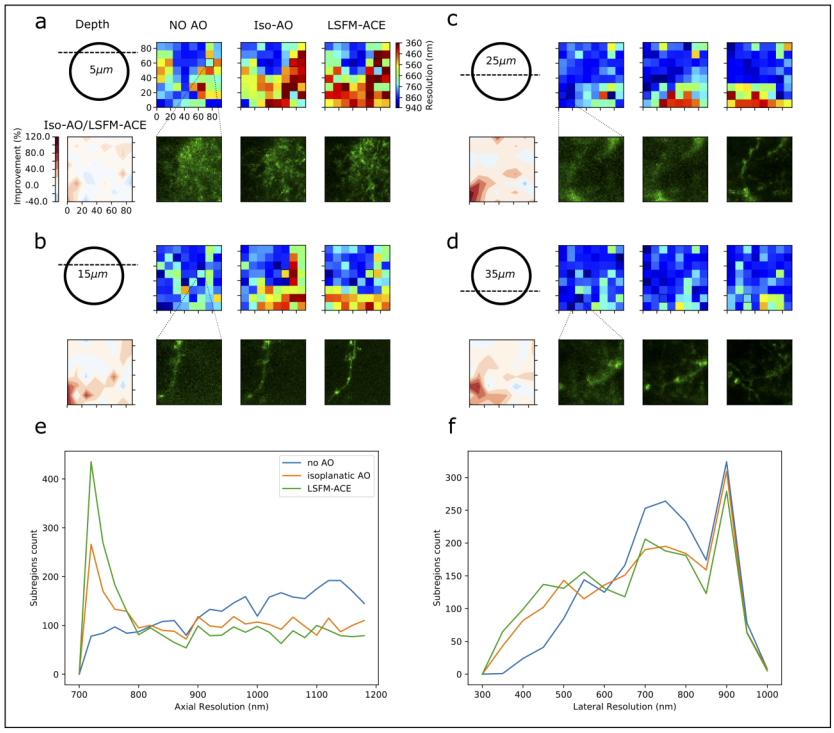

Fig. 4. Estimated resolution. Results of Fourier Ring Correlation of single subregions in the data presented in Fig. 3. **a-d** Distribution of estimated resolution, , relative improvement of anisoplanatic correction compared to traditional AO, and a selected subregion detail for the image acquired at 5 to 35μm depth in the sample e-f Histogram of the distribution of axial and lateral resolution amongst subregions in the volume at depths higher than 10μm.

Optics EXPRESS

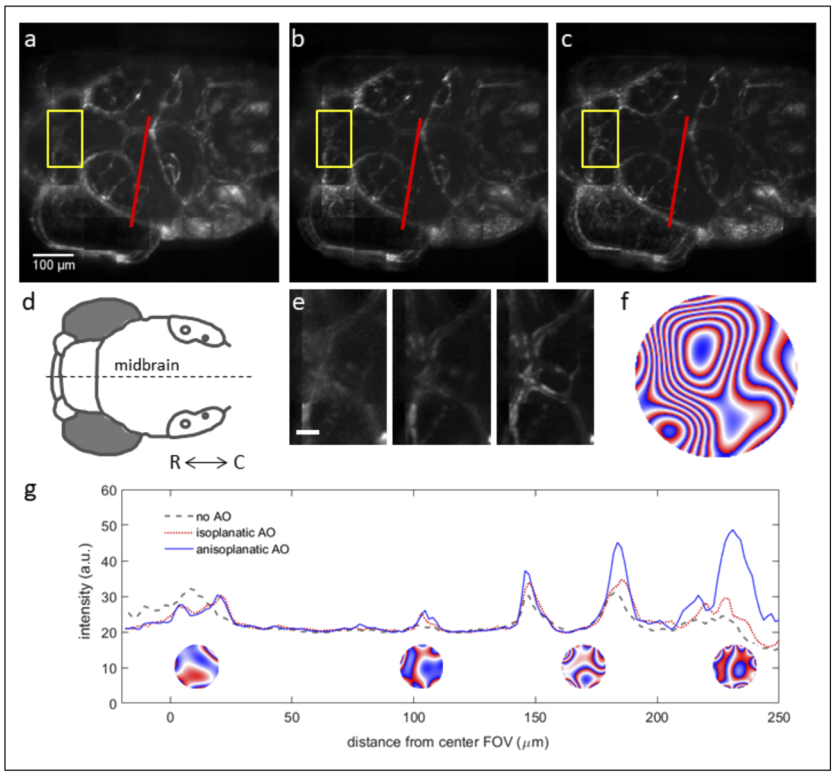

Fig. 5. Maximum instensity projections of zebrafish images. Maximum intensity projections of images from a fixed 4 dpf larva expressing GFP in blood vessels is shown with **a** no aberration corrections; **b** isoplanatic corrections; **c** LSFM-ACE images. **d** Schematic of zebrafish head indicating rostral (R) – caudal (C) axis. **e)** Detail from forebrain region indicated by box in panel a. Scale bar is 20μm. **f** Wrapped isoplanatic aberration corrected in b. **g** Comparison of line profiles (indicated by red line in b) shows that the LSFM-ACE method particularly improved features far from the FOV center, in this case making smaller vessels visible in the optic tectum. Inset images show wrapped corrections applied to corresponding individual isoplanatic patches.

Optics EXPRESS

7. Discussion

In this paper, a new method for the correction of sample induced aberrations in confocal microscopy has been presented, presenting the first reported simultaneous correction of anisoplanatic aberrations introduced by three dimensional samples. The presented method exploits computer generated holography to illuminate the sample with a lattice of independently corrected excitation spots, which can be raster scanned through the sample to generate a parallelized confocal microscopy image. A deformable mirror is used to perform conventional isoplanatic adaptive optics on the fluorescence light. The results presented show how the isoplanatic nature of conventional correction approaches severely limits the performance of adaptive imaging systems in biological samples, and the introduction of anisoplanatic correction greatly enhances the image quality.

If compared to existing anisoplanatic correction methods (e.g. conjugate adaptive optics [8,10], multiplexed pupil [7] or time multiplexing [6]), LSFM-ACE provides the first real parallelized correction without time multiplexing, and with none of the tradeoffs between correction resolution and isoplanatic patch size presented by previously reported methods. The only effective lower limit to the isoplanatic patch size is due to cross talk between out of focus excitation when imaging densely labeled thick specimens, and is equivalent to the excitation spacing limit in any parallelized acquisition system (e.g. spinning disk microscopy [20], programmable array microscopy [21]) Moreover, by conjugating both phase modulators to the pupil plane of the objective, the optical system is simpler to design, implement, align and operate. The method allows high resolution, optical sectioning imaging in relatively thick and turbid media potentially providing, in specific cases, an alternative to multiphoton microscopy when the intrinsic advantages of linear excitation are needed (e.g. higher resolution, lower cost, higher spectral separation of excitation.). As a collateral, but useful addition, due to the independent correction of excitation and fluorescence light, LSFM-ACE provides a form of correction of chromatic aberrations between excitation and emission wavelengths.

The two main limitations of the reported implementation of the technique lie in the size of the field of view, and in the image acquisition speed which, while being comparable to those of a traditional laser scanning microscope, are quite limited, especially if compared to existing parallelized acquisition techniques such as spinning disk microscopy [22] or multiphoton multifocal microscopy [23]. These drawbacks are anyway purely technical, and technology enabling their improvement is rapidly evolving. As an example, SLMs recently made available commercially have resolutions which would allow an up to 4-fold extension of the field of view on both axes with minimal difference in acquisition speed, while arrays of fast photodetectors are quickly developing and could improve the speed of parallelized acquisition systems such as the one described in this manuscript by up up to two orders of magnitude.

It is to be noticed how, while the method only corrects anisoplanatically the excitation light path, ensuring that a fully corrected excitation beam scans the sample greatly increases the image resolution. It can be assumed that uncorrected anisoplanatic aberration in the fluorescence light path only produces a degradation in detected light intensity, but does not affect the image resolution. The signal limitation due to limited correction of fluorescence light could be provided in the future by implementation of the method in multiphoton microscopy, provided that the isoplanatic correction applied to fluorescence light is sufficient for separation of the signals from different excitation spots on the camera.

Finally, while the reported measurements were provided for low-order aberrations, the presented method, being based on a high-resolution corrector, could allow higher order aberrations correction, up to the limit of scattering compensation [11]. This would, however, require faster refreshing SLM technologies, faster optimization algorithms [24], and some form of high order correction of fluorescence light.

Optics EXPRESS

8. Methods

Drosophila samples preparation. We imaged Drosophila brains containing native GFP and mRFP signal. First, the brains were dissected in PBS (1.86 mM NaH2PO4, 8.41 mM Na2HPO4, and 175 mM NaCl) and fixed using a ice-cold 4% paraformaldehyde solution for an additional 60 min at room temperature. The brains were washed 3 times for 10 minutes in PBS solution with 0.1 % Triton X-100 and again 2 times for 10 minutes with PBS. The native fluorescence signal was boosted by immunostaining against GFP and mRFP as previously described in [25]; primaries at 1:2,000 for 2 overnights at 4 C and secondaries at 1:500 for 1 overnight at 4 C. We used anti-GFP (chicken, abcam13970) and anti-DsRed (Rabbit, Clontech 632496, 1:2,000).

Zebrafish samples preparation. Zebrafish embryos expressing GFP in blood vessels were obtained from an incross of Tg(flk1:eGFP) fish with *nacre* background. Larvae were euthanized at 4 days past fertilization, fixed in 2% paraformaldehyde solution with 0.1 M PHEM buffer for 1 hour, rinsed 3x in PBS, and stored in PHEM buffer at 4 C until imaging.

Funding

European Research Council (339681, 695140).

Acknowledgments

The authors would like thank of W.J.M. van Geest and C.J. Slinkman for technical contributions, and L. Gouweleeuw and the zebrafish facility staff at Leiden University for preparing the zebrafish samples.

Disclosures

The authors declare no conflicts of interest.

References

1. N. Ji, "Adaptive optical fluorescence microscopy," Nat. Methods **14**(4), 374–380 (2017).
2. M. J. Booth, M. A. Neil, R. Juškaitis, and T. Wilson, "Adaptive aberration correction in a confocal microscope," Proc. Natl. Acad. Sci. **99**(9), 5788–5792 (2002).
3. D. C. Johnston and B. M. Welsh, "Analysis of multiconjugate adaptive optics," J. Opt. Soc. Am. A **11**(1), 394–408 (1994).
4. E. Marchetti, N. N. Hubin, E. Fedrigo, J. Brynnel, B. Delabre, R. Donaldson, F. Franza, R. Conan, M. L. Louarn, C. Cavadore, A. Balestra, D. Baade, J.-L. Lizon, R. Gilmozzi, G. J. Monnet, R. Ragazzoni, C. Arcidiacono, A. Baruffolo, E. Diolaiti, J. Farinato, E. Vernet-Viard, D. J. Butler, S. Hippler, and A. Amorin, "Mad: the eso multiconjugate adaptive optics demonstrator," in *Adaptive Optical System Technologies II*, vol. 4839 (International Society for Optics and Photonics, 2003), pp. 317–328
5. J. Thaung, P. Knutsson, Z. Popovic, and M. Owner-Petersen, "Dual-conjugate adaptive optics for wide-field high-resolution retinal imaging," Opt. Express **17**(6), 4454–4467 (2009).
6. T. l. Liu, S. Upadhyayula, D. E. Milkie, V. Singh, K. Wang, I. A. Swinburne, K. R. Mosaliganti, Z. M. Collins, T. W. Hiscock, J. Shea, A. Q. Kohrman, T. N. Medwig, D. Dambournet, R. Forster, B. Cunniff, Y. Ruan, H. Yashiro, S. Scholpp, E. M. Meyerowitz, D. Hockemeyer, D. G. Drubin, B. L. Martin, D. Q. Matus, M. Koyama, S. G. Megason, T. Kirchhausen, and E. Betzig, "Observing the cell in its native state: Imaging subcellular dynamics in multicellular organisms," Science **360**(6386), eaaq1392 (2018).
7. J. H. Park, L. Kong, Y. Zhou, and M. Cui, "Large-field-of-view imaging by multi-pupil adaptive optics," Nat. Methods **14**(6), 581–583 (2017).
8. J. Mertz, H. Paudel, and T. G. Bifano, "Field of view advantage of conjugate adaptive optics in microscopy applications," Appl. Opt. **54**(11), 3498–3506 (2015).
9. H. P. Paudel, J. Taranto, J. Mertz, and T. Bifano, "Axial range of conjugate adaptive optics in two-photon microscopy," Opt. Express **23**(16), 20849–20857 (2015).
10. J. H. Park, W. Sun, and M. Cui, "High-resolution in vivo imaging of mouse brain through the intact skull," Proc. Natl. Acad. Sci. **112**(30), 9236–9241 (2015).
11. I. M. Vellekoop and A. Mosk, "Focusing coherent light through opaque strongly scattering media," Opt. Lett. **32**(16), 2309–2311 (2007).
12. M. Plöschner, B. Straka, K. Dholakia, and T. Čižmár, "Gpu accelerated toolbox for real-time beam-shaping in multimode fibres," Opt. Express **22**(3), 2933–2947 (2014).

Optics EXPRESS

13. R. Di Leonardo, F. Ianni, and G. Ruocco, "Computer generation of optimal holograms for optical trap arrays," Opt. Express **15**(4), 1913–1922 (2007).
14. P. Pozzi, L. Maddalena, N. Ceffa, O. Soloviev, G. Vdovin, E. Carroll, and M. Verhaegen, "Fast calculation of computer generated holograms for 3d photostimulation through compressive-sensing gerchberg–saxton algorithm," Methods Protoc. **2**(1), 2 (2019).
15. T. D. Visser and S. H. Wiersma, "Electromagnetic description of image formation in confocal fluorescence microscopy," J. Opt. Soc. Am. A **11**(2), 599–608 (1994).
16. D. Wilding, P. Pozzi, O. Soloviev, G. Vdovin, and M. Verhaegen, "Adaptive illumination based on direct wavefront sensing in a light-sheet fluorescence microscope," Opt. Express **24**(22), 24896–24906 (2016).
17. P. Pozzi, O. Soloviev, D. Wilding, G. Vdovin, and M. Verhaegen, "Optimal model-based sensorless adaptive optics for epifluorescence microscopy," PLoS One **13**(3), e0194523–15 (2018).
18. D. Débarre, M. J. Booth, and T. Wilson, "Image based adaptive optics through optimisation of low spatial frequencies," Opt. Express **15**(13), 8176–8190 (2007).
19. T. J. Gould, D. Burke, J. Bewersdorf, and M. J. Booth, "Adaptive optics enables 3d sted microscopy in aberrating specimens," Opt. Express **20**(19), 20998–21009 (2012).
20. T. Shimozawa, K. Yamagata, T. Kondo, S. Hayashi, A. Shitamukai, D. Konno, F. Matsuzaki, J. Takayama, S. Onami, H. Nakayama, Y. Kosugi, T. M. Watanabe, K. Fujita, and Y. Mimori-Kiyosue, "Improving spinning disk confocal microscopy by preventing pinhole cross-talk for intravital imaging," Proc. Natl. Acad. Sci. **110**(9), 3399–3404 (2013).
21. P. Pozzi, D. Wilding, O. Soloviev, H. Verstraete, L. Bliek, G. Vdovin, and M. Verhaegen, "High speed wavefront sensorless aberration correction in digital micromirror based confocal microscopy," Opt. Express **25**(2), 949–959 (2017).
22. A. Nakano, "Spinning-disk confocal microscopy–a cutting-edge tool for imaging of membrane traffic," Cell Struct. Funct. **27**(5), 349–355 (2002).
23. J. Bewersdorf, R. Pick, and S. W. Hell, "Multifocal multiphoton microscopy," Opt. Lett. **23**(9), 655–657 (1998).
24. H. R. Verstraete, S. Wahls, J. Kalkman, and M. Verhaegen, "Model-based sensor-less wavefront aberration correction in optical coherence tomography," Opt. Lett. **40**(24), 5722–5725 (2015).
25. E. Perisse, D. Owald, O. Barnstedt, C. B. Talbot, W. Huetteroth, and S. Waddell, "Aversive learning and appetitive motivation toggle feed-forward inhibition in the drosophila mushroom body," Neuron **90**(5), 1086–1099 (2016).